Investigation of Immiscible and Miscible Foam for Enhancing Oil Recovery

R. Farajzadeh,[†,‡] A. Andrianov,[†] and P. L. J. Zitha*[,†,‡]

Shell International Exploration and Production, Rijswijk, The Netherlands, and Delft University of Technology, Delft, The Netherlands

We report the study of flow of CO_2 and N_2 foam in natural sandstone cores containing oil with the aid of X-ray computed tomography. The study is relevant for enhanced oil recovery (EOR). The cores were partially saturated with oil and brine (half top) and brine only (half bottom) to mimic the water−oil transition occurring in oil reservoirs. The CO_2 was used either under subcritical conditions ($P = 1$ bar) or under supercritical (immiscible ($P = 90$ bar) and miscible ($P = 137$ bar)) conditions, whereas N_2 remained subcritical. Prior to gas injection the cores were flooded with several pore volumes of water. In a typical foam experiment water flooding was followed by the injection of 1−2 pore volumes of a surfactant solution with alpha olefin sulfonate (AOS) as the foaming agent. We visually show how foam propagates in a porous medium containing oil. At low-pressure experiments ($P = 1$ bar) in the case of N_2, weak foam could be formed in the oil-saturated part. Diffused oil bank is formed ahead of the foam front, which results in additional oil recovery, compared to pure gas injection. CO_2 hardly foams in the oil-bearing part of the core, most likely due to its higher solubility. Above the critical point ($P = 90$ bar), CO_2 injection following the slug of surfactant reduces its mobility when there is no oil. Nevertheless, when the foam front meets the oil, the interface between gas and liquid disappears. The presence of the surfactant (when foaming supercritical CO_2) did not affect the oil recovery and pressure profile, indicating the detrimental effect of oil on foam stability in the medium. However, at miscible conditions ($P = 137$ bar), injection of surfactant prior to CO_2 injection significantly increases the oil recovery.

1. Introduction

A problem associated with many secondary and tertiary gas (e.g., CO_2, N_2, steam, air) injection projects is the inefficient gas utilization, and poor sweep efficiency and oil recovery due to viscous fingering and gravity segregation (see Figure 1). The fingering and segregation result from high gas mobility (displacing phase) compared to oil and water (displaced phase); i.e., gas density and viscosity are much lower than those of oil and water. Unfavorable mobility ratios lead to even more severe channeling in heterogeneous reservoirs. Consequently, the drive fluid does not contact a large part of the reservoir and the volumetric sweep efficiency of the reservoir remains poor.[1]

The alternation slugs of water and gas, i.e., water alternating gas (WAG), has been common practice to obtain better mobility ratios and improve sweep efficiency.[2−4] Nonetheless, WAG can eventually suffer from viscous instabilities and gravity segregation and, therefore, has not always been a successful method for controlling the gas mobility.[5]

The addition of surfactant to water results in a process called surfactant alternating gas (SAG). By foaming the gas (see Figure 1) and, thus, reducing its mobility, especially in the swept or high permeability parts of the reservoir, one can potentially overcome the problems encountered in WAG.[6−12] Foaming of the injected gas reduces its mobility by immobilizing or trapping a large fraction of the gas without compromising its efficiency. As a result, part of the gas is diverted into the oil-rich part of the reservoir and oil recovery is enhanced. Note that the mechanism of oil displacement by foam differs from that for surfactant flooding due to the presence of the gas phase. Foam can affect the oil recovery in two ways: (1) by stabilizing the displacement process by increasing the displacing fluid (gas) viscosity and (2) by reducing the capillary forces via reducing the interfacial tensions due to the presence of surfactant. The latter mechanism is dominant in alkaline surfactant foams (ASF), where the interfacial tension between the fluids drops more drastically.[13] In addition to these two important mechanisms, since the gas is in more contact with oil, the interfacial mass transfer between gas and oil will also play an important role in mobilizing the oil in place by dissolution, viscosity reduction, and swelling.[14] Diffusion induced bulk transport[15] and, in the case of CO_2, natural convection further assist these processes by enhancing the transfer rate through the liquid−gas interfaces.[16,17]

One concern with the application of SAG (foam) as an enhanced oil recovery (EOR) method is the longevity of foam when it contacts the crude oil. Many experiments, both in bulk and in porous media, have shown the detrimental effect of oil on foam stability.[18−22] Mainly based on bulk experiments, three major mechanisms have been considered for the antifoaming property of the dispersed oils: (1) aqueous film thinning rate during oil droplet entry, (2) oil spreading on the water surface, and (3) thin water film bridging.[23,24] An oil droplet must first

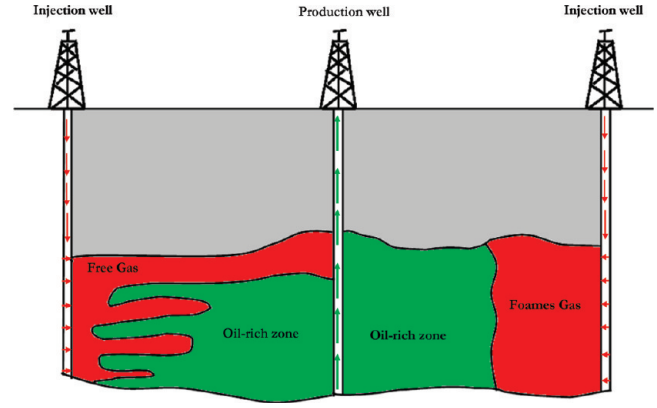

Figure 1. Schematic of gas flooding vs SAG (or foam) flooding. Foaming of the gas modifies its profile by lowering gas mobility.

* To whom correspondence should be addressed. E-mail: p.l.j.zitha@tudelft.nl.
[†] Shell International Exploration and Production.
[‡] Delft University of Technology.

10.1021/ie901109d
Published on Web 12/29/2009

enter the gas−water surface to affect the foam stability. The feasibility of droplet entry to the gas−water interface, $E_{o/w}$, can be evaluated by an expression proposed by Harkins:[25]

$$E_{o/w} = \sigma_{gw} + \sigma_{ow} - \sigma_{go} \quad (1)$$

In this equation σ is the interfacial tension and subscripts "w", "o", and "g" stand for water, oil, and gas, respectively. It is favorable for oil to enter the gas−water interface when $E_{o/w} > 0$. When an oil droplet enters the gas−water interface, it might spread over the surface. This again depends on the interfacial tensions of the phases. The spreading coefficient, $S_{o/w}$, is defined as

$$S_{o/w} = \sigma_{gw} - \sigma_{ow} - \sigma_{go} \quad (2)$$

The spreading does not occur when the spreading coefficient is negative. The bridging coefficient, B, is defined as a criterion for the effect of oil bridging on foam stability:

$$B = \sigma_{gw}^{\ 2} + \sigma_{ow}^{\ 2} - \sigma_{go}^{\ 2} \quad (3)$$

Negative values of B indicate that films are stable. Note that foam behavior in porous media, due to the presence of sand grains, and also confined and nonuniform pore geometry, can be rather different from that of bulk foams.[20] As a consequence, the direct use of the results obtained from bulk foam experiments is debatable. In porous media, critical (or limiting) capillary pressure is usually a measure of foam stability. In other words, if the water saturation is below or oil saturation is above certain values, foam will collapse. Thus, foam in the absence of oil may behave differently from foam in the presence of oil. Yet, if we assume that the right formulation of surfactant is designed for an enhanced oil recovery (EOR) foam, it is not clear how long foam can propagate in the reservoir (considering the well spacing) and by which mechanism oil will be produced.

The objective of this paper is to study the effect of foam injection on oil recovery using two gases, namely N_2 and CO_2. Therefore, we describe experiments in which we inject a slug of surfactant followed by CO_2 or N_2 to a core containing waterflood residual oil. With the aid of computed tomography (CT) images we show how foam will look when it contacts oil in the porous medium. The structure of the paper is as follows: section 2 describes the experimental setup and the experimental procedures. Section 3 presents the experimental results of two sets of experiments. The first set of the experiments is performed at atmospheric pressure and at room temperature of $T = 20$ °C for both N_2 and CO_2. The second set of experiments is conducted above the critical point of CO_2 under immiscible ($P = 90$ bar) and miscible ($P = 137$ bar) conditions at $T = 50$ °C. We end the paper with concluding remarks.

2. Experimental Details

2.1. Materials. 2.1.1. Chemicals. The surfactant used for foaming was alpha olefin sulfonate, AOS (Stepan Co., USA). This surfactant is anionic and was used as received without any further purification. The general structure of olefin surfactants is $R-SO_3^-Na^+$, where R represents the hydrophobic group. In our case the number of the carbon atoms in the surfactant structure is 12 and the molecular weight of the surfactant is $M_w = 273$ g/mol. A fixed active surfactant concentration of $c_{AOS} = 0.50$ wt % was used in all experiments. Sodium chloride (NaCl) was used to make the brine. The concentration of NaCl was at fixed value of 0.5 M (∼3 wt %) in all experiments reported here. All the solutions were prepared with deionized water (pH 6.8 ± 0.1). In order to increase the CT attenuation of the solutions, 10 wt % sodium tungstate was added. One test was done without this salt to evaluate its effect on foam performance. The result showed no significant difference from the experiment with the salt. However, its possible effects on the foaming behavior of the gases may need a more detailed investigation.

Table 1. Entering, Spreading, and Bridging Coefficients Calculated from Interfacial Tension (eqs 1−3) for Isopar H

property	value
$E_{o/w}$	1.10
$S_{o/w}$	1.403
B	304.95

Table 2. Properties of Sandstone Cores (Porous Media)

permeability [mD]	porosity [%]	diameter [mm]	length [mm]	pore volume [mL]	main composition
1010	22 ± 0.2	40 ± 1	170 ± 2	42.5 ± 0.5	quartz

2.1.2. Oil. Isopar H (ExxonMobil Chemical) was used as oil phase in the experiments. The density and viscosity of this synthetic oil at 25 °C are 0.76 g/cm^3 and 1.35 cP, respectively. Isopar H is a mixture of C_9-C_{11} with an unknown composition. The minimum miscibility pressure (MMP) of the CO_2/Isopar H system was estimated to be in the range of ∼100−115 bar at $T = 50$ °C, using different correlations.[26] The entering, spreading, and bridging coefficients were calculated for the system of Isopar H and AOS solution. Interfacial tensions were measured at the room temperature of 20 °C and atmospheric pressure. The gas above oil and water was air. The results are presented in Table 1. The positive values of $E_{o/w}$ and $S_{o/w}$ indicate that that Isopar H enters the gas−water interface and spreads over it. The positive value of B implies that films are unstable due to the bridging of oil droplets.

2.1.3. Gases. The gases used to carry out the experiments were 99.98% pure CO_2 and N_2.

2.1.4. Porous Media. The porous medium used was consolidated, quasi-homogeneous, and quartz-rich Bentheimer sandstone. The main properties of the porous medium are presented in Table 2. The permeability was calculated from the pressure data of a single-phase (brine) flow (with a known flow rate) through the core, and the porosity was determined from the CT data. The radiuses of the pore throats are mainly in the range 10−30 μm.

2.2. Experimental Setup. The schematic of the experimental setup is shown in Figure 2. It consists of four parts: injection unit (IU), test unit (TU), pressure controlling unit (PCU), and data acquisition system (DAS).

2.2.1. Injection Unit. In order to ensure the supply of the gas at a constant rate, the gas flow rate is controlled by a high-precision needle valve (for low-pressure experiments) and an ISCO pump (for high-pressure experiments) and monitored by using a gas flow meter. Two high-precision double-effect piston displacement pumps (Pharmacia P 500) are used to inject the brine, the surfactant solution, and the oil at constant rates.

2.2.2. Test Unit. In the test unit, the sample core is placed inside a cylindrical coreholder. The coreholder is made of polyethylene ether ketone (PEEK), which combines good mechanical properties and a low X-ray attenuation. The core holders were placed vertically on the platform of the CT scanner apparatus and kept in place using a poly(methyl methacrylate) (PMMA) stand. The foam is introduced from the bottom of the core, and the liquid production is collected in scaled tubes at the outlet of the core holder. Two high-precision pressure transducers are placed at the inlet and the outlet to monitor the pressure drop along the core.

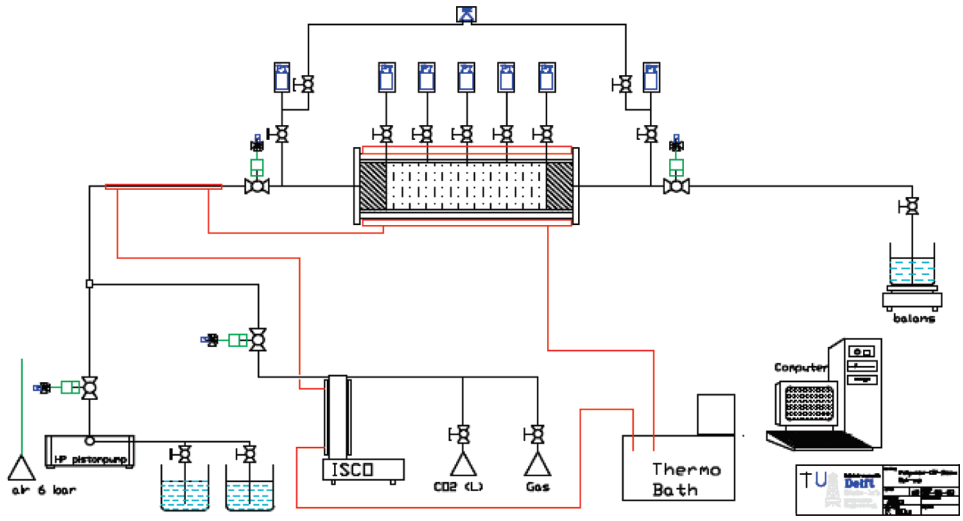

Figure 2. Schematic of the foam setup. It consists of four major units: injection unit (pumps), test unit (the porous medium), pressure controlling unit, and data acquisition system.

Table 3. Settings of CT Scan Measurements

parameter	CT scan setting
energy levels [keV]	140
current [mA]	250
slice thickness [mm]	3
number of slices	4
filter	B40-medium

2.2.3. Pressure Control Unit. The pressure control part connects to the outlet of the core. By using a back-pressure regulator and a manometer, we can measure different pressures in the system. The data acquisition system records gas and liquid injection rates, pressures, and the liquid production data automatically. All experiments are conducted under isothermal conditions. The low-pressure experiments were done at room temperature of $T = 20$ °C, and the high-pressure experiments were performed at $T = 50$ °C.

The core-flood setup was placed on the couch of the CT scanner. The PEEK core holder is positioned vertically, perpendicular to the surface of the table, to minimize the effects of gravity segregation. The third-generation SAMATOM Volume Zoom Quad slice scanner from the Dietz laboratory was used in our work. The imaging settings used in our experiments are listed in Table 3. The X-ray tube of the CT scanner is operated at a nominal voltage of 140 kV and current of 250 mA. The thickness of a CT slice is 3 mm, and one series of scan includes four slices. In the calculations the slice corresponding to the center of the core was used.

2.3. Calculation of Oil Saturation. The following equation is used to compute the oil saturation S_o, from the measured attenuation coefficients (HU), eliminating the contribution of the rock by subtraction

$$S_o = \frac{1}{\varphi}\left(\frac{HU - HU_{wet}}{HU_o - HU_w}\right) \quad (4)$$

where the subscripts "wet", "o", and "w" stand for brine (or surfactant) saturated core, oil, and brine, respectively. The accuracy of eq 4 is within ±2%. This equation is valid when only two phases, i.e., water and oil or water and gas, are present in porous medium.

2.4. Experimental Procedure. 2.4.1. Saturation with Brine. The core was flushed with CO_2 for at least 30 min to replace the air in the system. Afterward, at least 20 pore volumes of brine at the flow rate of $q_w = 2$ mL/min were injected into the system while the back pressure was set to $P_b = 20$ bar. Therefore, all CO_2 present in the core was dissolved into the brine and carried away. This is also confirmed by the CT images.

2.4.2. Drainage. After the core was saturated with brine, it was flushed with a known amount of oil ($q_o = 0.5$ mL/min) to displace the brine. To overcome the gravity and consequently fingering (instability) effects, the oil was injected from the top.

2.4.3. Imbibition. The brine was injected into the core ($q_w = 2$ mL/min) from the bottom until no more oil was produced and the pressure drop along the core was constant within the accuracy of our measurements.

2.4.4. Surfactant Injection. After water flooding the core, 1−2 pore volumes of surfactant solution was injected ($q_s = 2$ mL/min) into the porous medium from the bottom of the core. The surfactant solution contained 0.5 wt % AOS surfactant and 3.0 wt of NaCl salt.

2.4.5. Foam (Gas) Injection. The gas was injected into the core previously flushed with the surfactant solution from the bottom of the core; i.e., foam was injected in SAG mode and generated in situ.

3. Results and Discussion

3.1. Drainage and Imbibition. The images and corresponding saturation profiles of drainage and imbibition stages are similar for all the experiments, and therefore only one typical data set is presented in Figures 3 and 4. Figure 3a shows how oil (yellow) injected downward drains brine (red) from the upper part of the core, whereas Figure 3b illustrates how brine injected upward displaces oil. It is clear that in both cases the gravity stabilizes the flow, as oil density (0.76 g/cm^3) is lower than water density (1.0 g/cm^3). The corresponding oil saturations, calculated from the images using eq 4, are shown in Figure 4a and 4b, respectively. The profiles in Figure 4a are reminiscent of a Buckley−Leverett theory displacement.

The accuracy of the last points (at $X = 17$ cm) is poor due to the beam hardening effects at the edges of the core holder.[27] Note that the residual oil saturation might vary slightly in different axial slices made from the core as Figure 4 shows the calculated saturation only for the central part of the core. The oil distribution in the core may also vary slightly from experiment to experiment, but the overall trend is reproducible.

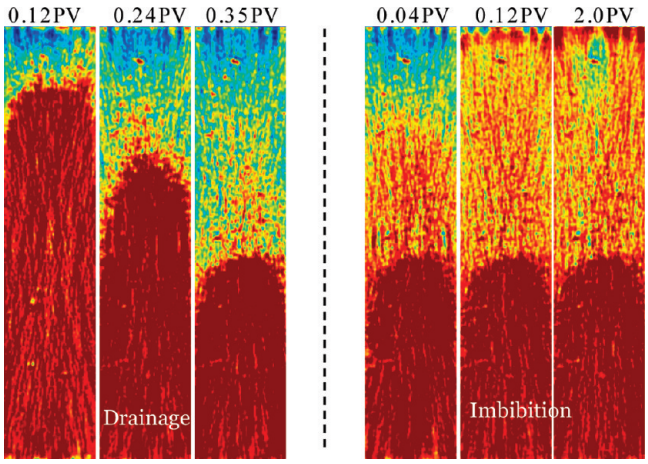

Figure 3. CT images of an example of the drainage step (a, left) and imbibition step (b, right) of the experiments. Oil (Isopar H) is injected from top of the core initially saturated with brine (drainage). Afterward, brine is injected from the bottom (imbibition).

3.2. Low-Pressure Foam. During primary and secondary recovery, oil is trapped in the reservoir pore structure. The degree of trapping is a function of the capillary number, which is defined as

$$N_c = \frac{v\mu}{\sigma} \tag{5}$$

The aim of any recovery method is to increase the oil production by increasing the capillary number. Within the realistic flow rates this is possible by (1) reducing the mobility of the displacing fluid (i.e., increasing its viscosity) and (2) reducing the interfacial tensions. Interfacial tensions between oil and water do not change drastically with addition of *conventional* surfactants, and therefore, for foam to be an efficient *drive fluid*, its apparent viscosity should be higher than that of oil when it contacts the oil-rich zone. This requires oil-tolerant foams to be generated in porous media. In this section we study the mechanisms by which oil is produced when (N_2 or CO_2) foam is injected into a core containing water-flood residual oil.

3.2.1. CT Scan Images. Figure 5a and Figure 5b present the CT images of the central part of the N_2 and CO_2 experiments, respectively. The time of each image is also given in pore volumes (PV), i.e., the ratio between the cumulative volume of injected fluids and the volume of the pore space in the porous medium. The volume of the injected gas in the experiments is calculated at the inlet pressure, and therefore the dimensionless times expressed as PV in this paper are also at the inlet conditions. In these experiments N_2 was injected at 0.50 standard mL/min (~2 ft/day) and CO_2 was injected at a flow rate of 0.75 mL/min into the core initially flooded with 1.0 PV of the surfactant solution (SAG scheme). The higher flow rate of CO_2 was chosen to compensate partially the effect of dissolved gas. The blue, red, and orange colors represent the foam (gas and surfactant solution), water $S_w = 1$, and water-flood residual (or more accurately remaining) oil S_{or}, respectively. The green part constitutes the three-phase region. The remaining oil fractions of the core are given in Table 4 for both experiments after water flooding. The general features of both experiments in the water-saturated part (red) are similar to the experiments discussed in ref 28; i.e., N_2 almost immediately penetrates the core while a considerable amount of CO_2 is injected into the core before it becomes visible. As time passes, the upper part of the core becomes reddish due to the fact that foam displaces the aqueous phase from the water-saturated part toward the core outlet in a way typical of a high-viscosity fluid displacing a liquid. After about 0.20 PV the N_2 reaches the oil−water contact, while this time is more than 1.0 PV for CO_2. This is likely due to the higher solubility of CO_2 in water as discussed in ref 28.

3.2.2. Production Data. The CT images in Figure 5 clearly show that when N_2 reaches the oil−water contact the foam front is destroyed, at least partially. This leaves a higher liquid saturation at the oil−water contact due to capillary effects (Since foam is destroyed, its apparent viscosity decreases and viscous forces are no longer dominant over capillary forces and hence oil remains trapped.) Part of the gas bypasses the oil, and the other part channels through the oil-containing part of the core. The gas breakthrough occurs at about 0.30 PV in the N_2 experiment. This suggests that the presence of oil significantly increases the gas phase mobility by destroying the foam.

Another intriguing feature in the N_2 experiment is the existence of a liquid bank ahead of the gas (foam) front. This becomes more obvious from Figure 6, where the oil and water production data are presented. It turns out from these plots that at the time N_2 appears in the entire length of the core (~0.40 PV) large amounts of liquid (water and oil) are produced. More strictly speaking, almost all of the oil (within the accuracy of our measurements) is produced at this time, emphasizing the fact that foam pushes the oil out of the core (see Figure 7).

Similar to N_2, when CO_2 reaches the oil−water contact (OWC), the sharp interface between the gas and the liquid is destabilized, but to a smaller extent. CO_2 is not as dispersed as N_2 in the oil phase. Instead, similar to the water-saturated part of the core, CO_2 dissolves into oil and moves slower than N_2, possibly due to its higher solubility in both water and oil compared to N_2. The oil production in the CO_2 experiment is less than in the N_2 experiment. Most likely in the CO_2 experiment there is much less foam generation in the oil-containing part because of the (1) higher solubility of CO_2, which leaves less free CO_2 gas for foaming, and (2) detrimental effect of oil on foam stability as discussed in the previous section. The small oil production in the CO_2 experiment can be attributed to the small amount of gas that is not dissolved.

3.2.3. Pressure Drops. Figure 8 shows the pressure drop along the water-saturated part (red line) and the entire core for N_2 foam (green line). It becomes evident from this figure that although a large fraction of the pressure drop is in the water part, injection of surfactant prior to N_2 slightly reduces its mobility despite the presence of oil. The pressure drop in the upper part of the core is less than one-third of the total pressure drop. The pressure profile obtained in this experiment for the water part is consistent with the pressure values presented in Figure 4 of ref 25.

Figure 9 compares the measured pressure drops versus dimensionless time (PV) of the two experiments. Unlike the oil-free experiments in ref 25, the difference between the pressure drops is not large and becomes insignificant after 1 PV. However, considering the differences in flow rates, it appears that N_2 injection builds up a higher pressure drop than CO_2 injection, in particular prior to gas breakthrough. This could explain the higher oil production for the N_2 experiment.

3.3. Supercritical CO_2 Foam. Several experiments (see Table 5) were carried out to investigate the effect of surfactant and foamed CO_2 on the oil recovery for the supercritical CO_2 EOR process. In these experiments the back pressure was set to 90 bar and the core was heated to 50 °C. The experimental

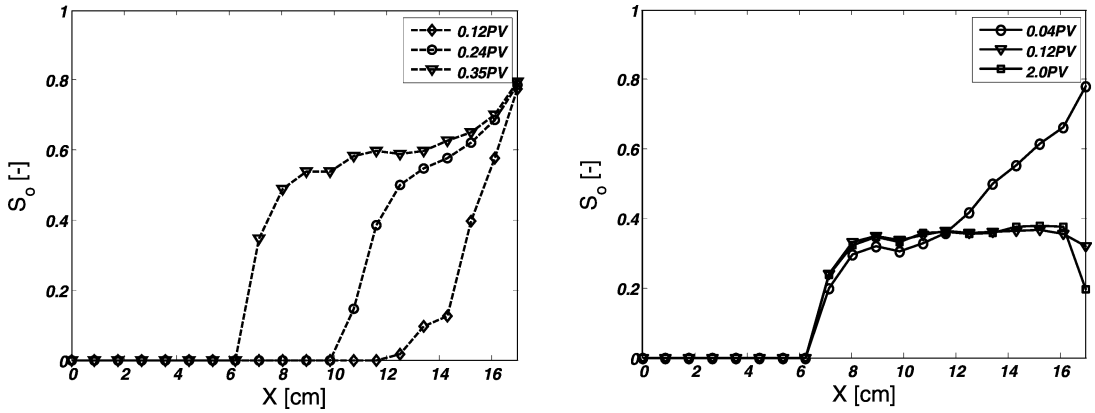

Figure 4. Oil saturation profiles for the drainage step (a, left) and imbibition step (b, right), calculated from CT profiles shown in Figure 6. *X* denotes the distance from the bottom.

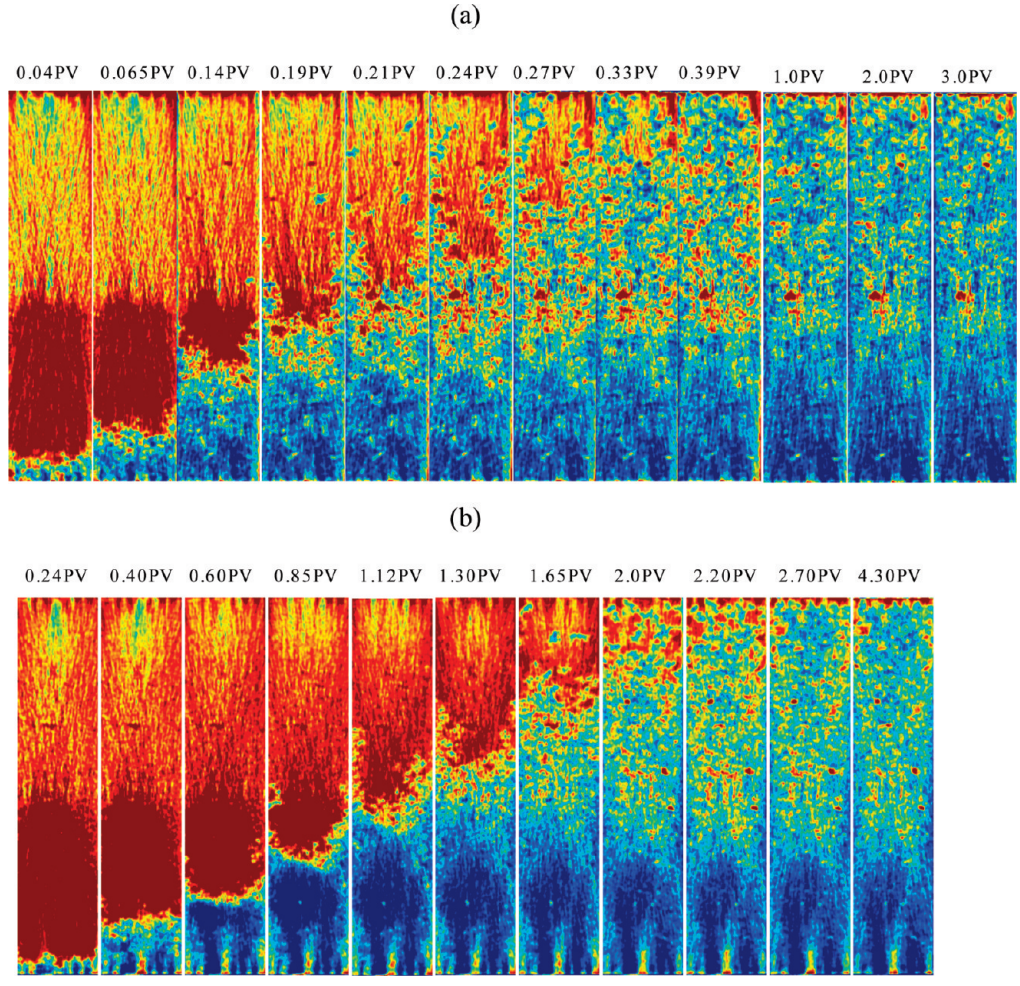

Figure 5. CT images of (a) N_2 and (b) CO_2 foam flow (blue, gas and surfactant solution) in a porous medium initially saturated with surfactant solution (red) and water-flood residual oil (orange, surfactant solution and oil) at $P = 1$ bar and $T = 20$ °C. The time of each image is shown in pore volumes of the injected gas. The green part after 1.30 PV constitutes the region where there are three phases. Gas is injected from the bottom.

Table 4. Summary of Experiments at Atmospheric Pressure and Room Temperature

gas	pressure [bar]	injected oil [mL]	water-flood S_{or} [%]	water-flood recovery [%]	surfactant recovery [%]	incremental oil recovery [%]	total recovery [%]
N_2	1.0	15.0	32 ± 2	47 ± 2	–	9.0 ±0.5	56 ± 2
CO_2	1.0	15.5	33 ± 2	46 ± 2	–	4.0 ± 0.5	50 ± 2

procedure and materials were similar to those for the low-pressure experiments.

3.3.1. CO_2 Gas Flooding (EXP-01). In this experiment the core was first saturated with doped brine and then oil was injected from the top afterward. Figure 10 shows the CT images of the drainage and imbibition stages of this experiment. The comparison between the two slices on the left side of the dashed line shows the uneven distribution of oil in the core. After

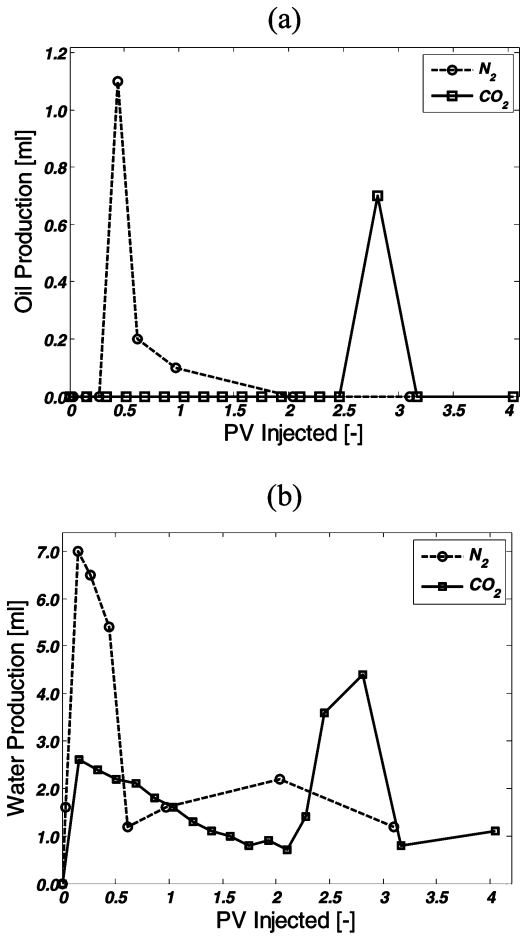

Figure 6. Production history of (a) oil and (b) water in N_2 and CO_2 SAG experiments at $P = 1$ bar and $T = 20$ °C. The first few points of the water production exhibit a starting-up effect.

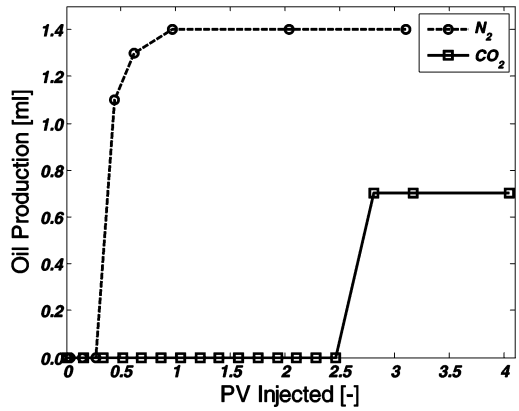

Figure 7. Cumulative oil production history of N_2 and CO_2 SAG experiments at $P = 1$ bar and $T = 20$ °C.

stopping oil injection the back pressure was increased to 90 bar and water was injected from the bottom into the core. The two pictures at the right side of Figure 10 show the fluid distribution inside the core. As can be observed, the air is trapped in some parts of the core and remains immobile. Figure 11 shows the calculated oil saturation along the core. From the CT calculations the maximum amount of oil inside the core is about 6.0 ± 0.2 mL after water flooding. This value is taken to compare the performance of CO_2 gas flooding and CO_2 foam flooding (EXP-02), which will be described below.

3.3.2. CO_2-Foam Flooding (EXP-02). Unlike the surfactant-free experiment (EXP-01), 1.5 PV of surfactant solution was

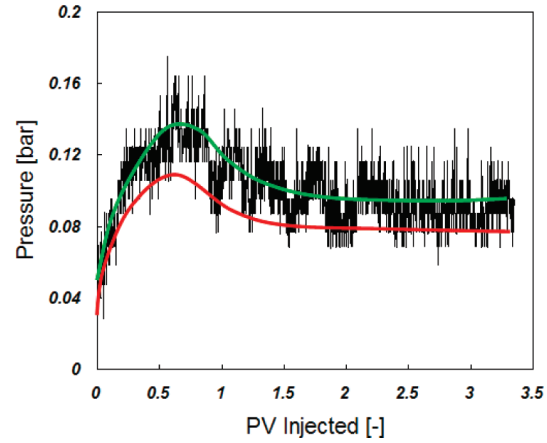

Figure 8. Pressure drop across the entire core (green) and in the water part of the core (red) for N_2 foam.

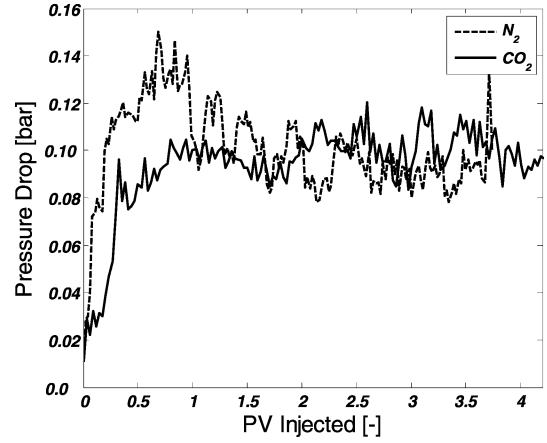

Figure 9. Pressure drop across the entire core for N_2 foam (dashed line) and CO_2 foam (solid line) at $P = 1$ bar and $T = 20$ °C.

injected into the core in the EXP-02 experiment after water flooding. Water flooding produced about 44% of the initial oil, which is similar to the recovery of the low-pressure experiments. The injection of surfactant did not recover additional oil since the reduction in interfacial tension is not substantial. Only for comparison purposes, in the following the same water-flooding recovery factor for both experiments (EXP-01 and EXP-02) will be assumed. The features of the two experiments are discussed in detail here below.

3.3.3. CT images. Figure 12 presents the CT images of the two experiments at corresponding times, i.e., pore volumes. As mentioned earlier, in the EXP-01 experiment (Figure 12a), CO_2 was injected into the core without surfactant (after water flooding) and in the EXP-02 experiment (Figure 12b) it was injected into the core, which was first flooded by surfactant solution. In both experiments, CO_2 was injected at the constant flow rate of 1.0 mL/min (~1.2 m/day). The blue, red, and orange colors represent the gas, water ($S_w = 1$), and water-flood residual oil (S_{or}), respectively. The green part constitutes the three-phase region. The images reveal that when CO_2 is injected into the core initially saturated with the brine (Figure 12a), there is no (clear) sharp interface between the gas and the brine. CO_2 forms channels through the brine only and reaches OWC at the time between 0.04 and 0.09 PV. When CO_2 is injected into the core initially saturated with the surfactant solution, a clear interface between the moving gas and liquid appears in the oil-free part. Foaming of CO_2 (Figure 12b) increases the time at which CO_2 reaches the OWC. However, comparing the two sets of images,

Table 5. Summary of Experiments with CO_2 at $T = 50$ °C

experiment	description	pressure [bar]	water-flood S_{or} [%]	water-flood recovery [%]	incremental oil recovery [%]	total recovery [%]
EXP-01	CO_2 gas	90	29 ± 2	44 ± 2	21 ± 1	65 ± 2
EXP-02	CO_2 foam	90	30 ± 2	44 ± 2	21 ± 1	65 ± 2
EXP-03	EXP-01 followed by CO_2 foam	90	–	–	19 ± 1	84 ± 2
EXP-04	CO_2 gas	137	33 ± 2	48 ± 1	28 ± 1	76 ± 2
EXP-05	CO_2 foam	137	31 ± 2	46 ± 2	40 ± 2	86 ± 2

it seems that injection of surfactant does not have a significant effect on the CO_2 transfer through the oil-saturated part. In both experiments there is no clear interface between the gas and liquid and the times required for CO_2 to travel from the OWC to the core outlet are comparable.

3.3.4. Pressure Profiles. Figure 13 plots the measured pressure drops versus dimensionless time (PV) for the two experiments. The maximum in both curves corresponds to the gas breakthrough time. The breakthrough happens later in the EXP-02 experiment due to the foaming of CO_2 in the first half of the core. Moreover, Figure 13 shows that injection of CO_2 into the core with surfactant (EXP-02 experiment) builds up a higher pressure, confirming the presence of foam. After CO_2 breakthrough there is no difference between the pressures of the two experiments, as the pressure curves overlap.

3.3.5. Production Profiles. Figure 14 presents the cumulative water and oil production for the two experiments. The small difference between the two water production curves can be attributed to the formation of foam. This slightly delays the water

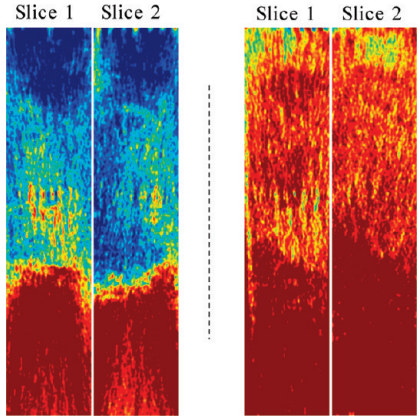

Figure 10. Two CT images of the drainage (left) and imbibition (right) stages of the EXP-01 experiment: Blue, green, and red represent gas, oil, and water, respectively. During the drainage part gas entered the core due to problems with the pump.

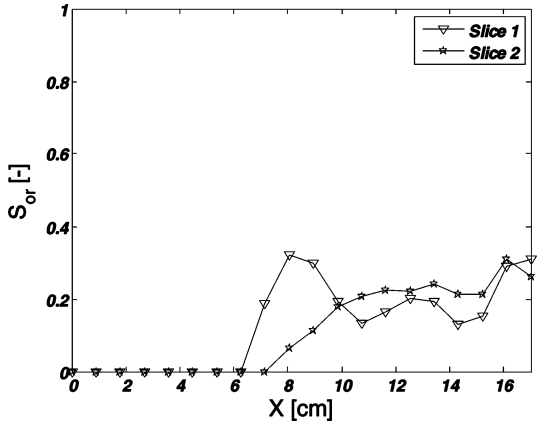

Figure 11. Oil saturation after water flooding in EXP-01. The total amount of oil inside the core is estimated to be about 6 mL from CT calculations.

(and oil) production and, more importantly, sweeps more water from the first half of the core, which explains the slightly higher water production in the EXP-02 experiment. The results are consistent with the experiments of ref 28. The ultimate oil recoveries in the two experiments are also similar. Given the fact that the amount of oil in the EXP-01 experiment was lower than that in the EXP-02 experiment prior to CO_2 injection, it can also be concluded that EXP-01 performs slightly better than the EXP-02 experiment. However, this difference can be due to the fact that we used two different cores in our experiments.

3.4. CO_2 Foam Following Gas Flooding. Due to severe channeling of the gas, further injection of CO_2 after about 1.0 PV did not recover measurable amounts of oil in the EXP-01 experiment. This experiment was continued by further injection of 1 PV of the surfactant solution followed by 1 PV of CO_2 to investigate whether foam could produce more oil after an inefficient gas-flood EOR. Figure 15 shows the pressure profile and production history of this experiment in terms of incremental oil recovery.

Injection of surfactant after 1.6 PV of CO_2 increases the pressure drop over the core because of the higher density and viscosity of the solution. Higher pressure drop over the core, more favorable displacement conditions, possible foaming of the existing CO_2 in the core, and lower viscosity of oil compared to its initial value (due to CO_2 dissolution) result in more oil production. About 9% of additional oil is recovered after 1 PV of surfactant injection. This was followed by another pore volume of CO_2 injection. Figure 16 shows the obtained CT images. The first two images are taken during surfactant injection. It is clear that surfactant solution displaces the gas from the lower section of the core. The middle images show the CO_2 injection. CO_2 foams in the water-filled part of the core (lower section) and delivers CO_2 into the upper part, which contains oil. Furthermore, as expected, the injection of CO_2 increases the pressure drop across the core due to formation of foam (or foamulsion[9]). The recorded pressure drop is higher than the pressure drop in the EXP-02 experiment because less oil is in the core and hence foam is more stable. The efficiency of foam can be evaluated by the mobility reduction factor (MRF) defined as

$$\mathrm{MRF} = \frac{(\Delta P/L)_f}{(\Delta P/L)_g} \tag{6}$$

where subscripts "f" and "g" stand for experiments with and without foam, respectively. From the pressure data of EXP-03, shown in Figure 15, injection of alternating slugs of CO_2 and surfactant provides effective MRF = 3.3. This increases the oil recovery by about 19% (9% after surfactant injection and 10% after CO_2 injection). The results of EXP-03 are significant as alternating slugs of CO_2 and surfactant recovers almost as much as the miscible CO_2 foam experiment (to be discussed in the next section). The experiment was continued by injection of surfactant, which resulted in fingering along the core (see Figure 16). The injection of surfactant after CO_2 did not recover additional oil.

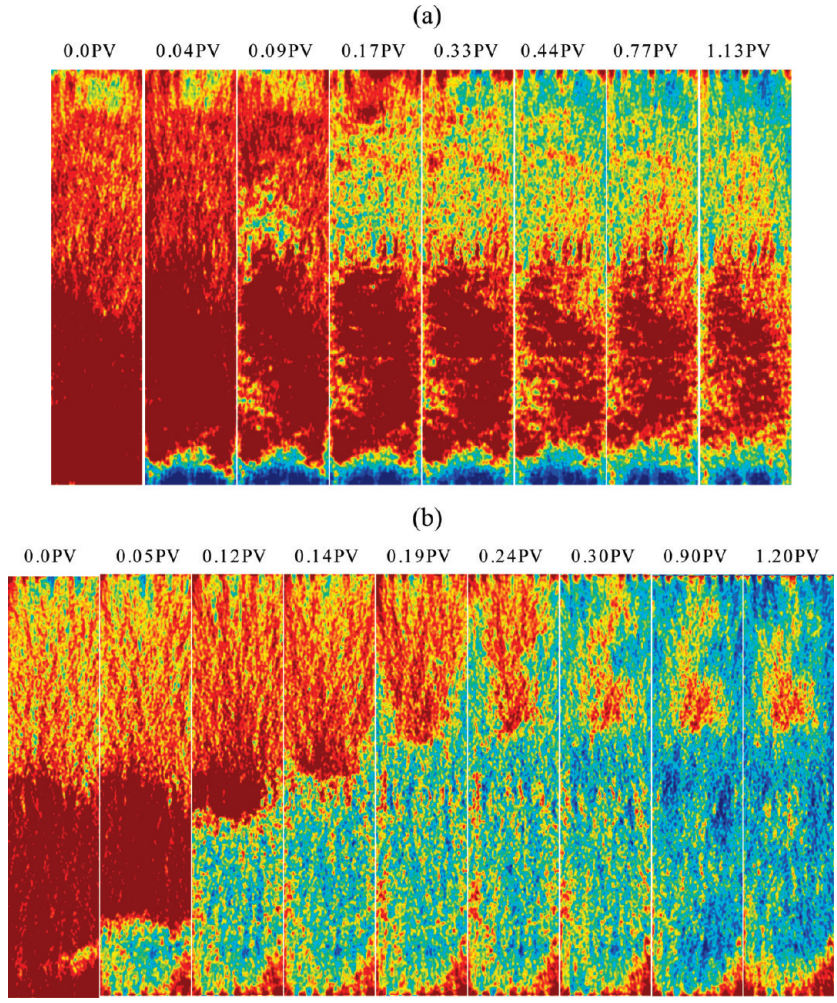

Figure 12. CT images of (a) EXP-01 and (b) EXP-02 in a porous medium initially saturated with brine or surfactant solution (red), gas (blue), and waterflood residual oil (orange) at $P = 90$ bar and $T = 50$ °C. The time of each image is shown in pore volumes of the injected gas. CO_2 is injected from the bottom.

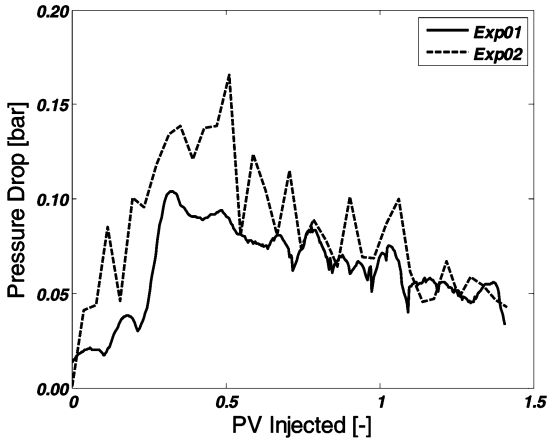

Figure 13. Pressure drop across the entire core for the EXP-01 and the EXP-02 experiments.

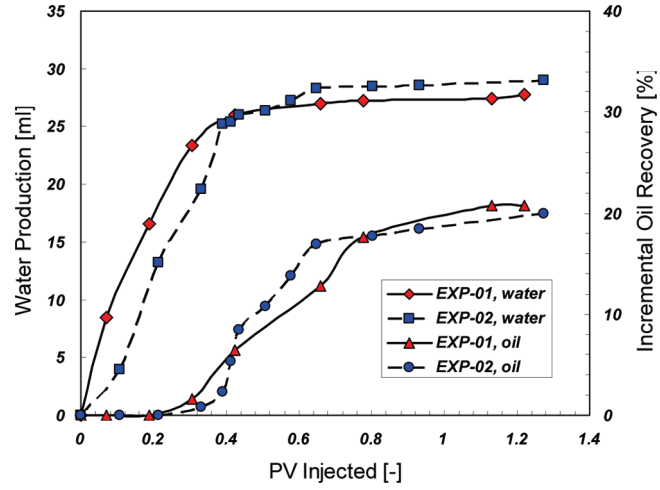

Figure 14. Cumulative water and oil production of EXP-01 and EXP-02 vs PVs of injected CO_2.

3.5. Miscible CO_2 Gas (EXP-04) and Miscible CO_2 Foam (EXP-05). Two experiments were done at the pressure of $P = 137$ bar and temperature of $T = 50$ °C with (EXP-05) and without (EXP-04) injecting 1.0 PV of surfactant solution prior to CO_2 injection. Figure 17 shows a significant increase in the oil production for EXP-05. The CT images of the experiment do not show a sharp front in the oil-saturated part of the core. Instead, similar to the previous experiments, there is a sharp front in the water-saturated part. This brings more CO_2 to the upper part of the core and, therefore, increases the CO_2 utilization efficiency; i.e., the amount of produced oil by a certain volume of CO_2 increases. The interesting feature of this experiment is that almost all of the oil is produced until the breakthrough of CO_2. This is an indication of formation of an oil bank ahead of the CO_2 front in the porous medium. In the EXP-04 experiment, the injected CO_2

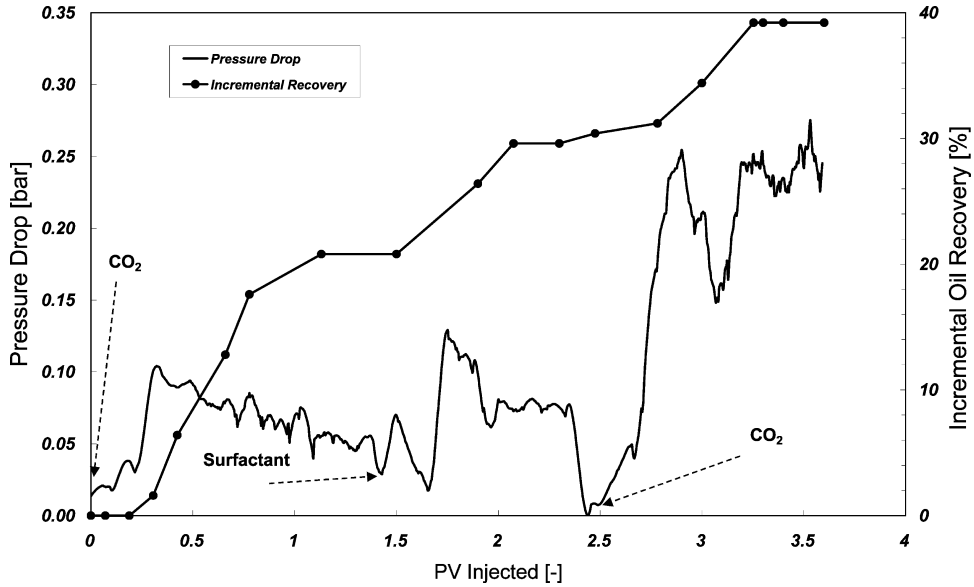

Figure 15. Pressure drop and incremental oil recovery by alternating slugs of surfactant and CO_2 (EXP-01 and EXP-03).

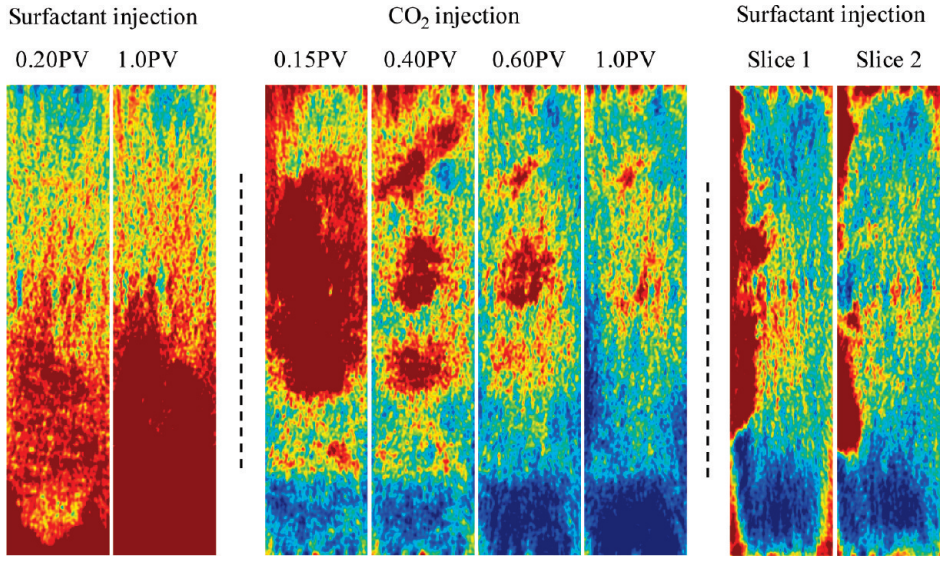

Figure 16. CT images of EXP-03 (surfactant solution (red), gas (blue), and gas−liquid mixtures (yellow)) at $P = 90$ bar and $T = 50$ °C. The time of each image is shown in pore volumes of the injected gas. Surfactant solution and CO_2 are injected from the bottom. The right images show the fingering of surfactant solution inside the core.

makes channels and breaks through earlier. However, due to favorable microscopic conditions, injection of CO_2 produces a considerable amount of oil.

It is possible to evaluate the CO_2 injection performance with the dimensionless tertiary recovery factor (TRF) defined as

$$\mathrm{TRF} = \frac{Q_o/Q_{S_{orw}}}{\mathrm{PV}_{g,inj}} \tag{7}$$

where Q_0 is the amount of produced oil, $Q_{S_{orw}}$ is the amount of oil that is left in the porous medium after water flooding, and $\mathrm{PV}_{g,inj}$ is the cumulative pore volume of the gas injected. This definition is adapted from ref 29 and normalizes the recoveries for comparison purposes. Figure 18 shows the normalized oil production for CO_2 experiments. Once again, this graph shows the significant improvement of CO_2 utilization efficiency for the oil recovery by foaming miscible CO_2. Note that, in the EXP-02 experiment at the OWC, CO_2 bypasses the oil and does

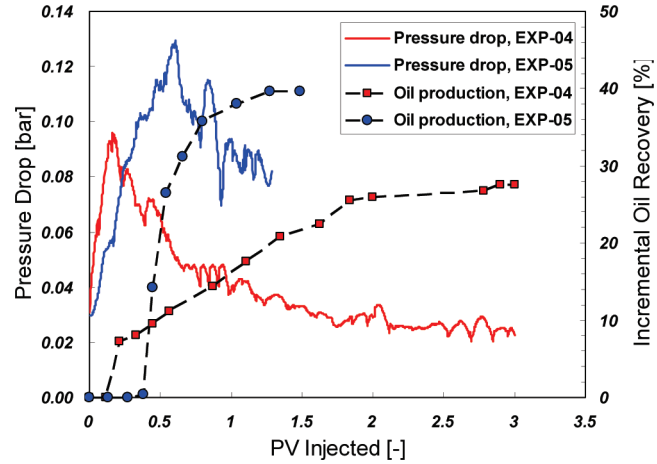

Figure 17. Pressure drop and oil production profiles for the EXP-04 and EXP-05 experiments.

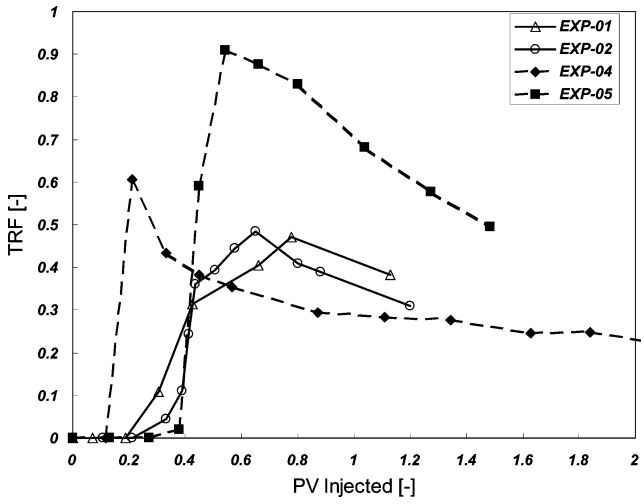

Figure 18. Tertiary recovery factor of EXP-01, EXP-02, EXP-04, and EXP-05 experiments calculated from eq 7 vs PVs of injected CO_2.

not contact oil. This is the main reason for the inefficiency of foam in the EXP-02 experiment.

4. Conclusions

We showed that, under our experimental conditions, injection of a foaming agent (namely AOS) prior to CO_2 injection above its minimum miscibility pressure (MMP) considerably increases the oil recovery and CO_2 utilization efficiency. However, below MMP CO_2 foam does not produce extra oil compared to tertiary CO_2 gas recovery. This is due to the fact that the presence of oil does not allow formation of foam in the porous medium. We observed that it is possible to reduce the mobility of subcritical and supercritical CO_2 when there is no oil present. Furthermore, we found that N_2 can form a weak foam zone in the presence of oil, ahead of which an oil bank moves toward the outlet of the porous medium. In this case, foaming of the gas enhances the oil recovery compared to gas injection.

On a reservoir scale, injection of surfactant followed by CO_2 injection (SAG foam) reduces the gas mobility in the regions where the oil saturation is very low. The reduction of gas mobility and blocking of the high permeable streaks will result in diversion of a portion of the injected gas into regions with higher oil saturation. Consequently, as more CO_2 contacts the oil in porous media and the pressure increases, extra oil will be produced by foaming CO_2. Therefore, foam will considerably improve the CO_2 utilization efficiency by reducing the amount of CO_2 required per unit of oil produced. Furthermore, delayed gas breakthrough and moderate gas production (lower gas to oil ratio) in the production wells will diminish the costs and problems associated with CO_2 handling. In conclusion, similar to steam foam, foaming of CO_2 can improve the ongoing (CO_2-) EOR processes and cannot be considered as a separate EOR process.

Acknowledgment

This research was carried out as part of a project funded by Delft Earth Research and Shell International Exploration and Production, Rijswijk. We thank Prof. Hans Bruining for a careful reading of the draft of the manuscript. We also thank the technicians of the Dietz laboratory of our faculty for their support.

Literature Cited

(1) Hinderaker, L.; Utseth, R. H.; Hustad, O. S.; Kvanvik, B. A.; Paulsen, J. E. Presented at the SPE European Petroleum Conference, Milan, Italy, Oct 22−24, 1996; SPE 36844.

(2) Christensen, J. R.; Stenby, E. H.; Skauge, A. Presented at the SPE International Petroleum Conference and Exhibition of Mexico, Vilahermosa, Mexico, March 3−5, 1998; SPE 39883.

(3) Hallam, R. J.; Ma, T. D.; Reinbold, E. W. Performance Evaluation and Optimization of The Kuparuk Hydrocarbon Miscible Water-Alternating-Gas Flood. Geological Society, London, Special Publications, 1995; Vol. 84, pp 153−164.

(4) Crogh N. A.; Eide, K.; Morterud S. E. Presented at SPE European Petroleum Conference, Oct 29−31, 2002, Aberdeen, United Kingdom; SPE 78348.

(5) Rao, D. N. *J. Can. Pet. Technol.* **2001**, *40* (2), 11–18.

(6) Hirasaki, G. J.; Lawson, J. B. *SPE J.* **1985**, (April), 175–190.

(7) Rossen, W. R. Foams in Enhanced Oil Recovery. In *Foams: Theory Measurement and Applications*; Prud'homme, R. K., Khan, S., Eds.; Marcel Dekker: New York City, 1996.

(8) Kovscek, A. R.; Radke, C. J. Fundamentals of foam transport in porous media. In *Foams: Fundamentals and applications in the Petroleum Industry*; ACS Advances in Chemistry Series 242; American Society: Washington DC, 1994.

(9) Wellington, S. L.; Vinegar, H. J. Surfactant-Induced Mobility Control for Carbon Dioxide Studied with Computerized Tomography. In *Surfactant Based Mobility Control—Progress in Miscible Flood Enhanced Oil Recovery*; Smith, D. H., Ed.; ACS Symposium Series 373; American Chemical Society: Washington, DC, 1988; pp 344−35.

(10) Du, D. X.; Naderi Beni, A.; Farajzadeh, R.; Zitha, P. L. J. *Ind. Eng. Chem. Res.* **2008**, *47*, 6298–6306.

(11) Xu, Q.; Rossen, W. R. Presented at the SPE Annual Technical Conference and Exhibition, Denver, CO, Oct 5−8, 2003; SPE 84183.

(12) Du, D. X.; Zitha, P. L. J.; Uijttenhout, M. G. H. *SPE J.* **2007**, (June), 245–252.

(13) Li, R. F.; Yan, W.; Liu, S.; Hirasaki, G. J.; Miller, C. A. Presented at the SPE/DOE Symposium on Improved Oil Recovery, Tulsa, OK, Apr 20−23, 2008; SPE 113910.

(14) Nobakht, M.; Moghaddam, S.; Gu, Y. *Fluid Phase Equilib.* **2008**, *265*, 94–103.

(15) Haugena, K. B.; Firoozabadi, A. *J. Chem. Phys.* **2009**, *130*, 064707.

(16) Farajzadeh, R.; Zitha, P. L. J.; Bruining, J. *Ind. Eng. Chem. Res.* **2009**, *48*, 6423–643.

(17) Farajzadeh, R.; Barati, A.; Delil, H. A.; Bruining, J.; Zitha, P. L. *J. Pet. Sci. Technol.* **2007**, *25* (12), 1493.

(18) Aveyard, R.; Binks, B. P.; Fletcher, P. D. I.; Peck, T. G.; Rucherford, C. E. *Adv. Colloid Interf. Sci.* **1994**, *48*, 93.

(19) Denkov, N. D. *Langmuir* **1999**, *15*, 8530.

(20) Bergeron, V.; Fagan, M. E.; Radke, C. J. *Langmuir* **1993**, *9*, 1704.

(21) Schramm, L. L. Foam sensitivity to crude oil in porous media. In *Foams: Fundamentals and Applications in the Petroleum Industry*; Schramm, L. L., Ed.; American Chemical Society: Washington, DC, 1994; Chapter 4, pp 165−197.

(22) Garrett, P. R. The mode of action of antifoams. In *Defoaming: theory and industrial applications*; Garrett, P. R., Ed.; Marcel Dekker: New York, 1993; pp 1−117.

(23) Nikolov, A. D.; Wasan, D. T.; Huang, D. W.; Edwards, D. A. Presented at SPE Annual Technical Conference and Exhibition, Oct 5−8, 1986; SPE 15443.

(24) Lau, H. C.; O'Brien, S. M. *SPE Reservoir Eng.* **1988**, *3* (Aug), 893.

(25) Harkins, W. D.; Feldman, A. *J. Am. Chem. Soc.* **1922**, *44*, 2665.

(26) Orr, F. M.; Silva, M. K. *SPE Reservoir Eng.* **1987**, (Nov), 479.

(27) Brooks, R. A.; Weiss, G. H.; Talbert, A. J. J. *Comput. Assisted Tomogr.* **1978**, *2*, 577.

(28) Farajzadeh, R.; Andrianov, A.; Bruining, J.; Zitha, P. L. J. *Ind. Eng. Chem. Res.* **2009**, *48*, 4542–4552.

(29) Kulkami, M. M.; Rao, D. N. *J. Pet. Sci. Eng.* **2005**, *48*, 1–20.

Received for review July 9, 2009
Revised manuscript received November 13, 2009
Accepted December 10, 2009

IE901109D